lubricants

MDPI

Article

Brake Wear Particle Emissions from Dry-Running Friction Systems: Influence of Operating Parameters and Friction Pairing Based on an Application-Oriented Extended Measurement Methodology

Francesco Pio Urbano *, Arne Bischofberger, Sascha Ott and Albert Albers

Institute of Product Engineering, Karlsruhe Institute of Technology, Kaiserstraße 10, 76131 Karlsruhe, Germany; arne.bischofberger@kit.edu (A.B.); sascha.ott@kit.edu (S.O.); albert.albers@kit.edu (A.A.)
* Correspondence: francesco.urbano@kit.edu

Abstract

Non-exhaust particulate emissions are expected to remain a relevant source of traffic-related air pollution, including an increase in electrified vehicle fleets. Particle formation results from tribological interactions and is influenced by both operating conditions and friction material system. This study presents an extended measurement methodology under application-relevant tribological conditions for the reproducible quantification of PM_{10} and $PM_{2.5}$ emissions from dry-running friction systems and applies it to a systematic investigation of operating parameter and friction pairing effects. A dry inertial brake test bench with an enclosed friction chamber and integrated aerosol measurement chain was used under controlled tribologically relevant conditions. Specific friction work and specific friction power were varied by adjusting sliding velocity, contact pressure, and inertial load. Six friction pairings, comprising four representative friction lining types combined with either C45 cast steel or GGG40 gray cast iron, were examined. In situ PM_{10} and $PM_{2.5}$ measurements were complemented by gravimetric wear and microstructural analyses. The results show that specific friction work has a direct influence on PM_{10} and $PM_{2.5}$ emissions, whereas the independent effect of contact pressure is secondary. Friction power exhibits material-dependent effects. Emissions also vary strongly with friction pairing, indicating that operating conditions and material system must be considered jointly when assessing low-emission brake systems.

Keywords: brake wear particles; PM_{10}; $PM_{2.5}$; friction work; friction power; non-exhaust emissions; dry-running friction systems; brake

Received: 21 March 2026
Revised: 12 April 2026
Accepted: 14 April 2026
Published: 17 April 2026

1. Introduction

1.1. State of the Art

Non-exhaust particulate matter (PM) emissions from road traffic are generated mainly by friction-induced wear processes in brakes and tires and represent a major public health concern due to their contribution to ambient PM exposure. In response to the documented adverse health effects of PM_{10} and $PM_{2.5}$, regulatory frameworks such as Euro 7 have increasingly expanded their scope beyond tailpipe emissions to explicitly address non-exhaust sources, which remain largely uncontrolled and highly relevant in urban environments. Beyond Europe, regulatory attention to non-exhaust emissions is also increasing, although the regulatory approaches remain heterogeneous. In the UNECE context,

a globally harmonized methodology for laboratory measurement of brake emissions has been established through UN GTR No. 24, and in 2026 this development was followed by a UN Regulation introducing standardized brake particle test methods and emission limits. In the United States, brake wear is not yet subject to harmonized federal vehicle-level PM limit values, but brake and tire wear are explicitly included in the EPA's MOVES5 emission model, while California and Washington already regulate brake-pad composition through restrictions and certification requirements, particularly for copper and other substances of concern. In Japan, national policy documents explicitly identify brake and tire dust as an increasingly relevant component of vehicle-related PM and link domestic policy development to ongoing UN harmonization activities. These developments underline that brake wear emissions are no longer only a European research topic, but an internationally emerging regulatory field. Brake wear has been identified as one of the dominant contributors to urban PM_{10} concentrations, with reported shares ranging from approximately 16% up to more than 50%, depending on traffic composition and local conditions [1–4].

Brake wear particles cover a broad size spectrum from coarse (PM_{10}) to fine ($PM_{2.5}$) and ultrafine fractions and exhibit a complex chemical composition. Their constituents include metallic oxides, carbonaceous phases, and inorganic additives originating from both pad and disc materials [5–8].

Several studies report that coarse brake wear particles are primarily generated by mechanical abrasion processes, whereas fine and ultrafine particles result from a combination of mechanical wear and thermally activated mechanisms, such as degradation and volatilization of organic binder components within the friction material [9–12].

Previous work by Sutschet et al. [13] formed the basis for the developed methodology of this paper. Sutschet et al. developed a validation environment using the IPEK-X-in-the-Loop approach (described in Section 2.2) for measuring particulate matter emissions from dry running brakes, and a methodology for connecting the loads experienced by the investigated friction pairs and the corresponding particulate matter emissions. While the methodology proposed by Sutschet et al. proved to be suitable for the investigation of fine particulate emissions, the influence of individual operational and material parameters was not examined. This paper builds upon the work done by Sutschet et al. by additionally focusing on particle morphology, particle chemistry, and operating parameters like sliding velocity, contact pressure, inertial load and friction energy dissipation through in situ and ex situ measurement techniques as described in Section 2.1. In contrast to Sutschet et al., these operating parameters will define the load cases instead of regulatory cycles, but the methodology used to gather the particulate matter for analysis will be the same.

The chemical composition of brake wear particles has been extensively investigated as an indicator of particle origin and formation mechanisms. For non-asbestos organic (NAO) and low-metallic brake pads, iron-rich particles dominate the coarse fraction, reflecting disc wear contributions, while finer particles frequently contain Fe oxides, Cu, Ti, Al, oxygen, and carbonaceous species [5,14]. Scanning electron microscopy (SEM) and energy-dispersive X-ray spectroscopy (EDX) analyses further show that brake wear particles are typically agglomerates consisting of multiple phases rather than single-element particles [7,9,15].

From a tribological perspective, brake wear particle generation is closely linked to the formation and evolution of the friction layer. Detached wear debris forms primary plateaus, while finer particles are compacted into secondary plateaus. The continuous formation, deformation, and disruption of this third-body layer is considered the dominant source of airborne wear particles during braking [11,14,16].

A large body of research literature demonstrates that operating parameters exert a strong influence on brake wear particle emissions. Sliding velocity and braking energy,

which together define the kinetic energy dissipated at the friction interface, are consistently reported as the most influential parameters governing PM_{10} and $PM_{2.5}$ emission levels [17,18]. As shown in Figure 1, $PM_{2.5}$ concentrations increase strongly with increasing initial speed, whereas the influence of brake pressure appears less pronounced. Overall, the literature indicates that speed-related effects dominate, while the impact of braking intensity is weaker and not always consistent across studies [1,19].

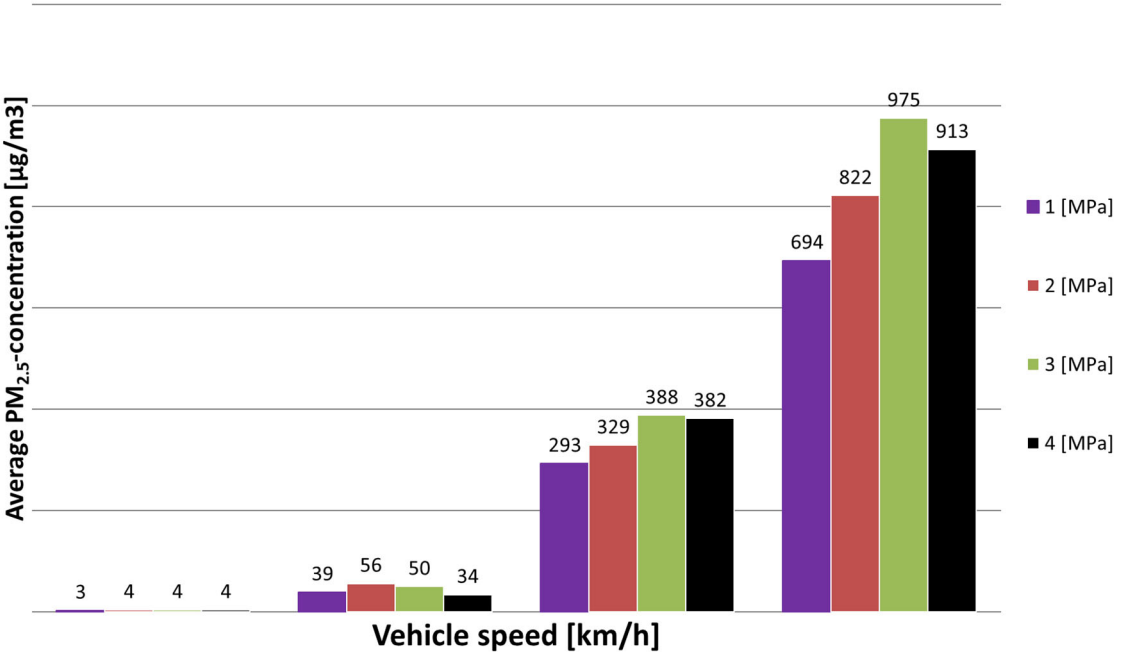

Figure 1. Effect of initial vehicle speed and brake pressure on $PM_{2.5}$ emissions (reproduced from [19]).

Contact pressure affects particle generation primarily by modifying the stability, compaction, and renewal rate of the friction layer rather than acting as an independent driver of emissions [10,16,20]. Temperature plays a secondary but important role, particularly for fine and ultrafine particles. Several studies report pronounced increases in $PM_{2.5}$ emissions once critical surface temperatures in the range of approximately 300–500 °C is exceeded, coinciding with thermal degradation of organic binder components [10,14,17,21].

In previous work, an inertial dry friction test rig with an enclosed friction contact and integrated fine dust measurement chain was developed to measure PM_{10} and $PM_{2.5}$ emissions under controlled conditions. This setup enables systematic variation in sliding velocity, contact pressure and flywheel mass, while evaluating friction coefficient, specific friction work, specific friction power and measuring airborne particle concentrations in real time. An extended methodology integrating in situ aerosol spectroscopy and ex situ cascade impaction, scanning electron microscopy (SEM) and energy-dispersive X-ray spectroscopy (EDX) has been applied to link operating conditions, emissions and wear mechanisms [13].

Three previous studies form the basis of the present work. The first systematically analyzed the influence of operating parameters on PM_{10} and $PM_{2.5}$ emissions from a sintered metallic friction system and identified that specific friction work directly influences PM_{10} and $PM_{2.5}$, while specific friction power showed material-dependent behavior. The second focused on developing and applying the extended measurement methodology and compared two organic ring-type friction pairings with different counter disc materials in terms of emissions, wear and particle chemistry. The third extended the investigation to six friction pairings using four pad materials in combination with C45 and GGG40 discs under six load stages [22–24].

Despite these advances, several fundamental gaps remain. Existing studies either investigate a limited subset of operating parameters for a given friction material or compare different materials under narrowly defined load scenarios. As a result, operating conditions and friction pairing are often treated separately, and their combined and interacting effects on PM_{10} and $PM_{2.5}$ emissions are not systematically resolved. In particular, the extent to which integrative tribological parameters such as specific friction work and friction power capture and unify the influence of sliding velocity, contact pressure, and inertial load across different material systems remains insufficiently clarified. From a methodological perspective, many experimental approaches focus predominantly on mass-based emission measurements or particle number concentrations without consistently linking these data to particle size fractions, morphology, chemical composition, and wear mechanisms within a single, coherent framework. Consequently, the mechanistic interpretation of measured emissions and their transferability across operating conditions and friction systems remain limited. There is therefore a clear need for an application-relevant experimental methodology that enables reproducible quantification of PM_{10} and $PM_{2.5}$ emissions while simultaneously providing access to size-resolved particle characteristics, chemical signatures, and tribological context. Moreover, such a methodology must be combined with a systematic experimental design that allows the influence of operating parameters and friction material systems to be evaluated in a consistent and physically interpretable manner. Addressing these gaps forms the basis and motivation for the present study.

1.2. Research Objectives and Scope

Building on the previous studies, the present article consolidates and synthesizes the experimental results into a comprehensive assessment of brake wear particle emissions from dry-running friction systems. A central objective is not only to analyze emission trends, but also to establish and apply a measurement methodology that enables a physically meaningful interpretation of particle formation mechanisms.

To this end, the work addresses one methodological and two scientific research questions.

Methodological Research Question:

How can an application-relevant experimental methodology be designed and applied to reliably quantify brake wear particle emissions in terms of particle mass (PM_{10}, $PM_{2.5}$), size fractions, and chemical composition under controlled but application-relevant operating conditions?

This methodological question is addressed by combining an enclosed dry inertial friction test rig with an integrated aerosol measurement chain and complementary ex situ analyses. Real-time PM_{10} and $PM_{2.5}$ mass concentrations are measured in situ, while cascade impaction followed by SEM and EDX analysis enables size-resolved investigation of particle morphology and elemental composition. Gravimetric wear measurements provide an additional integral metric linking emissions to material loss.

Based on this validated measurement approach, the following scientific research questions (RQ) are addressed:

RQ1: *How can a dry friction test bench be used to capture application-relevant brake wear particle emissions in a manner that is both quantitatively robust and mechanistically interpretable with respect to particle mass, size and chemical composition?*

RQ2: *How do the operating parameters of a dry-running brake friction system, specifically sliding velocity, contact pressure, and inertial load, govern the formation and emission intensity of PM_{10} and $PM_{2.5}$ brake wear particles, independent of material-specific effects?*

RQ3: *How do different friction material systems, including variations in friction pad formulation, reinforcement structure, constructive features, and counter disc material, affect PM_{10} and $PM_{2.5}$ emissions under identical operating conditions, acknowledging that geometry and material composition cannot be fully decoupled in the present test matrix?*

The objective of this paper is to answer these questions using a consistent experimental framework and to provide a tribologically grounded interpretation of the governing emission mechanisms. By explicitly linking operating parameters, material system properties, particle mass emissions, and chemical signatures, the study aims to contribute to the development of low-emission friction systems and to support future predictive modeling approaches for brake wear particle emissions.

2. Materials and Methods

2.1. Measurement Methodology and Experimental Concept

The objective of the applied measurement methodology is to enable a reproducible and application-relevant characterization of brake wear particle emissions under well-defined and systematically varied tribological boundary conditions. These boundary conditions include, among others, the initial temperature, sliding speed, normal load, and braking sequence, which govern the macroscopic system response while allowing the underlying physical mechanisms of wear and subsequent PM formation to occur naturally.

In contrast to purely regulatory or cycle-based approaches, the methodology is designed to relate imposed operating conditions and the resulting frictional energy input to the material response and particle formation processes. While quantities such as frictional power and frictional work are derived from measured signals and therefore subject to variations in the coefficient of friction, they provide a physically meaningful framework for comparing different operating conditions and identifying dominant trends in particle emission behavior. The methodological concept targets the comprehensive acquisition of particulate emissions with respect to

1. mass-related quantities (PM_{10} and $PM_{2.5}$);
2. particle size fractions;
3. particle morphology and chemical composition.

This multi-dimensional characterization is essential to distinguish between changes in emission intensity, shifts in particle size distribution and alterations in particle origin or formation mechanism.

To achieve this, the approach combines complementary in situ and ex situ measurement techniques. In situ aerosol measurements provide time-resolved mass concentrations of PM_{10} and $PM_{2.5}$ during each braking event, allowing transient emission behavior, peak values, and cumulative release to be captured under well-defined operating conditions. This data represents the cumulative amount of emitted airborne PM particles from the friction system, and form the quantitative basis for correlating emissions with operating parameters such as sliding velocity, contact pressure, inertial load, and frictional energy dissipation.

In parallel, ex situ particle collection enables a mechanistic interpretation of the measured emissions. Size-resolved particle fractions are deposited on dedicated substrates and subsequently analyzed with respect to morphology and chemical composition using scanning electron microscopy (SEM) and energy-dispersive X-ray spectroscopy (EDX). This dual strategy allows the origin of emitted particles to be assessed, for example by identifying disc-derived particles via iron-rich signatures or pad-related contributions via characteristic elemental markers. Beyond source attribution, the chemical composition of the particles is of particular relevance, as it directly influences both potential health effects and environmental impact, while also affecting technical interactions within the brake

system itself, such as friction behavior, wear progression, and surface transformations. Consequently, particle mass concentrations can be linked to specific wear mechanisms and material-related effects, rather than being treated as purely phenomenological quantities.

A key element of the methodology is the use of a dry-running friction pair test bench with an integrated flywheel to simulate inertial loads as seen in Figure 2. Compared to full-vehicle tests, roller dynamometers or standardized driving cycles, the inertial approach offers a substantially higher degree of control over individual operating parameters while maintaining mechanical relevance to braking processes. Unlike driving cycles, which superimpose numerous transient effects and boundary conditions, the inertial concept allows sliding velocity, contact pressure and inertial load to be varied independently and systematically under similar boundary conditions to reality (inertial loads, velocity profiles, contact pressure, etc.). This enables the isolation of the cause-and-effect relationships between operating conditions and particle emissions.

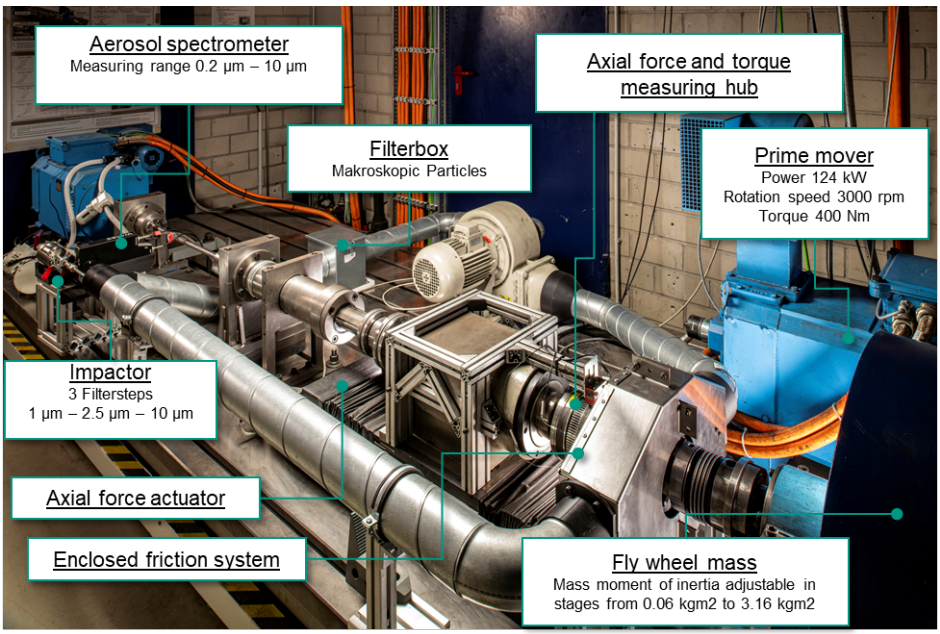

Figure 2. Dry-running friction pair test bench with flywheel module, drive unit, axial force actuator and enclosed friction chamber [24].

At the same time, the methodology deliberately exceeds the abstraction level of simplified pin-on-disc or small-scale tribometers. By employing representative contact geometries, realistic pressure and velocity ranges and repeated braking cycles, the approach ensures that third-body formation, friction layer evolution and wear particle generation occur under conditions that are comparable to real brake applications.

In this sense, the measurement methodology implicitly addresses RQ1: By combining brake application relevant inertial loads with integrated aerosol measurement and ex situ particle analysis, the presented methodology provides a consistent framework to answer this question and to support the investigation of both operating-parameter-driven and material-dependent effects on PM_{10} and $PM_{2.5}$ emissions.

2.2. Validation Environment

To implement the proposed measurement methodology under controlled yet application-relevant conditions, all experiments were conducted on a dry-running friction pair test bench developed at IPEK, Karlsruhe Institute of Technology (see Figure 2). The core components are a flywheel module, a variable-speed drive unit and an electromechanical axial force actuator. The flywheel module represents vehicle-equivalent inertias

up to 3 kgm^2, the drive unit provides rotational speeds up to 6000 min^{-1} with use of the belt-drive and the prime mover shown in Figure 2, and the axial actuator enables normal forces up to 10 kN.

These capabilities allow the realization of sliding velocities and contact pressures comparable to typical braking scenarios of passenger cars and industrial brakes.

2.3. Enclosure and Particle Sampling System

The friction contact (working surface pair: friction pad–counter disc (see Figure 3)) is completely enclosed and connected to a closed air-control system.

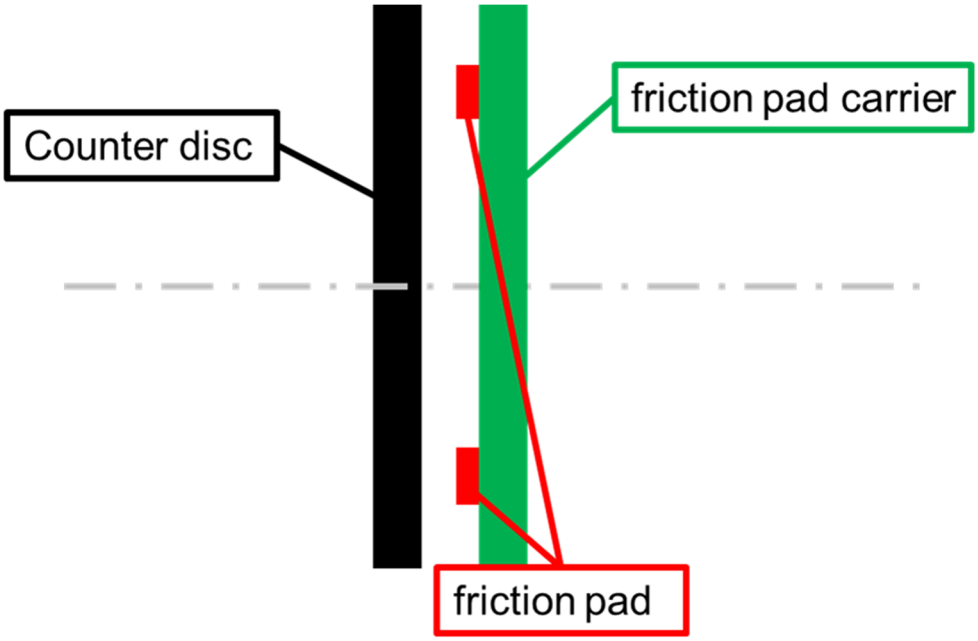

Figure 3. Schematic representation of friction contact between counter disc and friction pad.

A controlled volume flow transports the particles generated during braking from the friction chamber to a measurement and collection station. Flow straighteners and baffles are installed inside the enclosure to minimize disturbances of the third-body layer formation while ensuring efficient particle transport. The airflow around the tested friction pair is designed to not affect the thermal loads of the components as best as possible; i.e., the airflow does not cool the working surface pairs of the brake to a noticeable extent.

A calibrated real-time aerosol spectrometer system (Promo® 3000, PALAS GmbH, Karlsruhe, Germany) based on the optical light-scattering principle was used to determine airborne particle size distributions and the derived PM_{10} and $PM_{2.5}$ mass concentrations. The instrument was operated at a sample volume flow rate of 5 L min^{-1} and provided a temporal resolution of $\leq$1 s. In the sensor configuration used in this study, particles in the size range from 0.3 to 17 µm were detected and resolved into up to 128 size channels. Calibration was performed according to the manufacturer's specified procedure prior to the experiments. In parallel, a cascade impactor collects particles in size-resolved stages (PM_1, $PM_{2.5}$, PM_{10} and >PM_{10}) for ex situ analysis. The impactor substrates and filters are subsequently assessed by SEM and EDX to analyze particle morphology and chemistry. Larger particles are collected in a Petri dish located in the modified filter box and examined under a digital microscope. This setup enables the simultaneous quantification of PM_{10} and $PM_{2.5}$ mass concentrations as well as the collection of size-resolved particles for subsequent morphological and chemical analysis.

2.4. Evaluation Metrics and Measured Quantities

To answer the methodological and scientific research questions, the investigated variables were structured into measured quantities, geometric and defined boundary conditions, calculated tribological variables, and evaluation metrics used for interpretation.

During each braking cycle, braking torque, normal force, and rotational speed were recorded. Real-time PM_{10} and $PM_{2.5}$ mass concentrations were measured using the aerosol spectrometer. In addition, pad and disc mass were determined before and after each load stage to quantify gravimetric wear. Size-resolved particle samples were collected by cascade impaction and subsequently analyzed by SEM and EDX to assess particle morphology and chemical composition.

Geometric parameters such as effective friction radius and nominal contact area, as well as defined boundary conditions such as flywheel inertia and the temperature restart criterion, were treated as fixed parameters within each load stage.

Based on the measured quantities, several derived variables were determined. The friction coefficient was calculated from braking torque and normal force. Sliding velocity was derived from rotational speed and effective friction radius. Specific friction power was determined from the friction coefficient, normal force, and sliding velocity, and normalized by the nominal contact area. Specific friction work was determined by integrating friction power over one braking cycle and normalizing it by the nominal contact area. These calculated quantities represent the mechanical load state of the friction interface and serve as central variables for interpreting emission behavior.

For emission evaluation, cycle-averaged PM_{10} and $PM_{2.5}$ concentrations were calculated over 200 braking cycles for each combination of load stage and friction pairing. These averaged mass concentrations constitute the primary evaluation metrics of the study. In addition, peak concentrations were analyzed to characterize transient emission behavior, and cumulative sums over the complete sequence of cycles were evaluated to describe integral emission behavior.

Gravimetric wear of pad and disc was assessed as an integral material loss metric and compared with particle mass emissions to investigate potential correlations between wear progression and airborne particle release. SEM and EDX analyses were used qualitatively to identify morphological characteristics and elemental signatures of emitted particles, allowing differentiation between pad-derived and disc-derived material fractions.

This structured evaluation framework enables simultaneous assessment of particle mass, size fraction, morphology, chemical composition, and wear under controlled operating conditions. On this basis, the influence of sliding velocity, contact pressure, inertia, specific friction work, and specific friction power on PM_{10} and $PM_{2.5}$ emissions was systematically analyzed. Furthermore, emission levels and wear behavior were compared across different friction systems under identical operating conditions in order to isolate material-system effects.

2.5. Friction Pad Materials (A–F)

Four different friction pad materials were investigated each of which having a corresponding counter disc friction surface, leading to six friction pairings A–F.

All ring-shaped linings have a defined inner and outer diameter, ensuring known nominal contact area.

The exact diameters differ between the organic ring linings (A/B/C) and the wound linings (D/E), while F has a segment geometry similar to an automotive disc brake pad. Geometry and material composition are thus inherently coupled for each system and are not varied independently (see Table 1). Furthermore, friction pairs D and E have several spring elements (see Figure 4). The selected material systems allow a comparative

assessment of friction pairing effects under identical operating conditions, addressing Research Question 3.

Table 1. Overview of the friction pairings A–F: material class, geometry, reinforcement, spring features and intended application.

Friction Pairing	Material Class	Geometry	Reinforcement/ Structure	Spring Features	Nominal Contact Area/ Dimensions	Counter Disc Material	Intended Application/ Characteristics
A	Organic, mass-pressed	Ring-shaped	None	No	Inner Ø 140 mm, Outer Ø 160 mm	C45 steel	Baseline organic system; reference for organic–steel pairing
B	Organic, mass-pressed	Ring-shaped	None	No	Inner Ø 140 mm, Outer Ø 160 mm	GGG40 cast iron	Same friction pad as A; evaluates disc material influence
C	Organic, mass-pressed, high-abrasive	Ring-shaped	Increased abrasive fraction; elevated resin content	No	Inner Ø 140 mm, Outer Ø 160 mm	C45 steel	Higher hardness/stiffness; highest abrasion potential
D	Organic, wound lining	Ring-shaped	Glass fiber-reinforced	Yes (integrated spring elements)	Inner Ø 158 mm, Outer Ø 182 mm	C45 steel	Improved load distribution
E	Organic, wound lining	Ring-shaped	Glass fiber reinforced	Yes	Inner Ø 158 mm, Outer Ø 182 mm	GGG40 cast iron	Same design as D; comparison of steel vs. cast iron effects
F	Sintered metallic, bronze-based	Segment-shaped (pad-like)	Metallic matrix	No	Approx. 3026 mm^2	C45 steel	High thermal load capacity

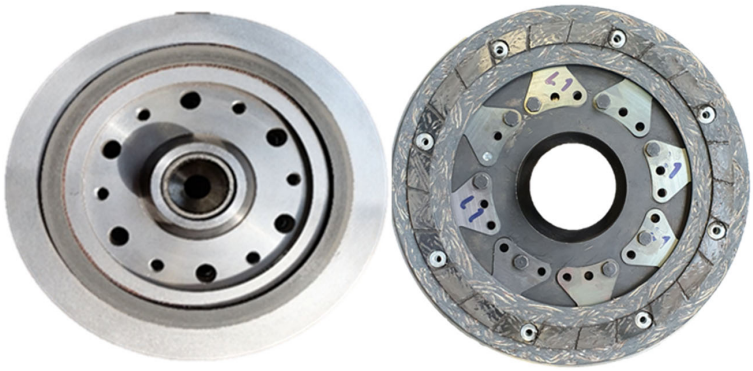

Figure 4. Ring shaped lining of friction pairing A and D/E from left to right.

2.6. Load Stages and Operating Parameters

Six load stages (L1–L6) were defined by systematic variation in sliding velocity, contact pressure and inertial load. Sliding velocity at the beginning of braking ranged between approximately 10 and 20 m s^{-1}, while nominal contact pressure was varied between about 0.3 and 0.7 MPa. The resulting specific friction work and specific friction power cover both basic load and partial misuse regimes and were determined as described in Section 2.4. The values listed in Table 2 are estimates based on the assumption of a constant friction coefficient, μ, and refer only to the initial values at t_0. For friction pairings D and E, comparable tribological load levels in terms of specific friction work and specific friction power were targeted using the same load-stage concept. Because these wound

lining systems differ in geometry and nominal contact area from pairings A to C, the corresponding nominal contact pressures and sliding velocities deviate slightly from the values listed in Table 2.

Table 2. Load stages L1–L6 with surface pressure, sliding speed, starting temperature, specific friction work and specific friction power for Pairing A/B/C.

Experimental Design	Unit	Run-In	L1	L2	L3	L4	L5	L6
surface pressure	MPa	0.30	0.64	0.35	0.40	0.19	0.64	0.35
sliding speed	m/s	10.0	13.0	19.3	13.0	19.3	13.0	19.3
starting temperature	°C	90.0	90.0	90.0	90.0	90.0	90.0	90.0
specific friction work	J/mm^2	1.1	1.5	1.2	2.1	2.5	2.7	3.2
specific friction power	W/mm^2	1.0	2.9	2.4	1.8	1.3	2.9	2.4

2.7. Test Procedure

For each friction pairing the following procedure was used:

- **Run-in:** 1000 braking cycles at the target load stage to stabilize the friction layer and achieve steady-state conditions.
- **Load stage:** 200 braking cycles at identical operating conditions.

Each braking cycle consisted of an acceleration phase to the target speed, a controlled brake application from constant speed to standstill, and a subsequent cooling phase. The cooling phase was initiated when the mean final temperature exceeded 90 °C; otherwise, the next braking cycle was started directly. For each friction pairing, a dedicated disc was used; the same disc was operated across all six load stages of that pairing. The brake pads were renewed before each load stage, after which the procedure described above was carried out. The pads then remained in place for the subsequent 200 acquisition cycles. The cascade impactor collection substrates were replaced after every load stage to enable subsequent SEM and EDX analyses of the size-resolved particle deposits. This procedure ensures steady-state friction conditions and reproducible emission measurements for each load stage and friction pairing.

3. Results

3.1. Influence of Operating Parameters on Emissions (RQ2)

The sintered metallic friction system F was investigated across the full range of load stages listed in Table 2 and, additionally, by means of an extended 2^3 design-of-experiments approach (Table 3) to isolate the influence of operating conditions. This approach allows a systematic variation in surface pressure, sliding velocity and inertial load, resulting in a wide range of specific friction work and specific friction power. As summarized in Table 3, the DOE matrix combines two levels of surface pressure, sliding velocity, and inertia. Each braking event was initiated at ambient conditions, and subsequent cycles were only started once the counterface temperature had decreased below 90 °C.

Table 3. Load stages L7–L14 with a 2^3 DOE-approach for friction pairing F.

Experimental Design	Unit	L7	L8	L9	L10	L11	L12	L13	L14
surface pressure	MPa	0.50	0.99	0.50	0.99	0.50	0.99	0.99	0.50
sliding speed	m/s	10.6	10.6	21.2	21.2	10.6	21.2	10.6	21.2
inertia	kgm^2	0.97	0.47	0.47	0.97	0.47	0.47	0.97	0.97
starting temperature	°C	90	90	90	90	90	90	90	90
specific friction work	J/mm^2	2.7	1.3	5.3	11.0	1.3	5.3	2.7	11.0
specific friction power	W/mm^2	2.1	4.2	4.2	8.4	2.1	8.4	4.2	4.2

Figure 5 shows the quasi-stationary mean PM_{10} and $PM_{2.5}$ mass concentrations of friction system F as a function of the measured specific friction work. The values were calculated from cycles 21 onward using consecutive 20-cycle block averages; error bars indicate 95% confidence intervals. The color coding represents the corresponding measured specific friction power.

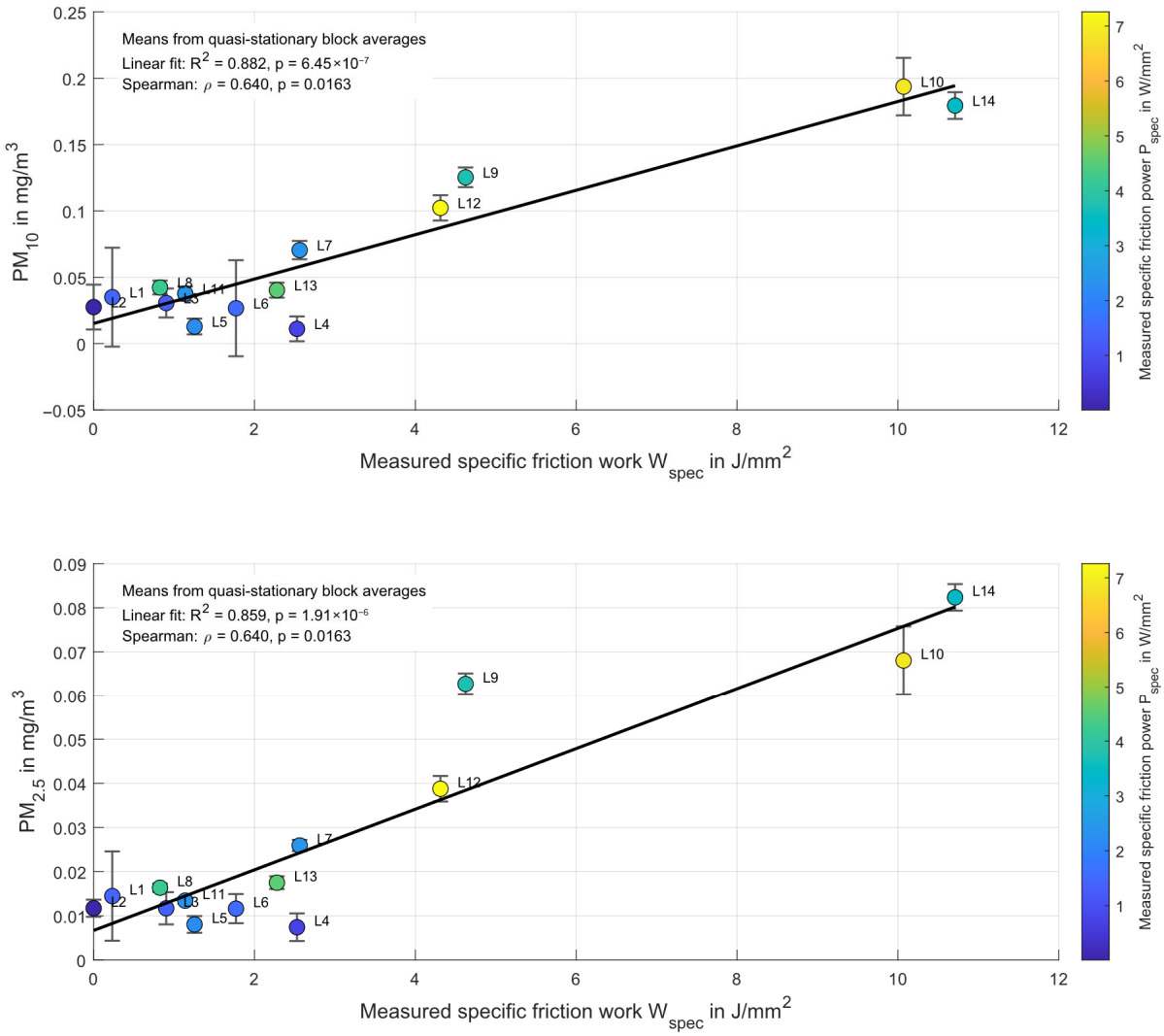

Figure 5. Quasi-stationary mean PM_{10} and $PM_{2.5}$ emissions of friction system F as a function of measured specific friction work. Means were calculated from cycles 21 onward using consecutive 20-cycle block averages; error bars indicate 95% confidence intervals. Point color indicates the corresponding measured specific friction power. Partly adapted from [24].

For both particle size fractions, the emission level increases clearly with increasing measured specific friction work across the investigated load stages. Load cases characterized by low friction work, such as L8 and L11, exhibit the lowest PM concentrations, whereas high-energy conditions, particularly L10 and L14, result in markedly elevated PM_{10} and $PM_{2.5}$ levels. To focus on the quasi-stationary emission behavior, the first 20 braking cycles were excluded from the evaluation. Under these conditions, a strong positive relationship between specific friction work and both PM fractions becomes evident. For PM_{10}, linear regression yields a coefficient of determination of $R^2 = 0.882$ with a highly significant positive slope ($p = 6.45 \times 10^{-7}$). For $PM_{2.5}$, the corresponding values are $R^2 = 0.859$ and $p = 1.91 \times 10^{-6}$. In addition, Spearman rank correlation confirms a significant monotonic association for both PM fractions ($\rho = 0.640$, $p = 0.0163$).

These findings indicate that, within the investigated operating range of friction system F, measured specific friction work provides a strong and physically meaningful descriptor of the PM_{10} and $PM_{2.5}$ emission levels.

When the quasi-stationary PM emissions of friction system F are evaluated as a function of the measured specific friction power (see Figure 6), a positive relationship is still observed for both particle size fractions, but the data are more scattered than in the corresponding representation over specific friction work. For PM_{10}, linear regression yields a coefficient of determination of $R^2 = 0.453$ with a significant positive slope ($p = 0.00838$), while Spearman rank correlation indicates a significant monotonic association ($\rho = 0.785$, $p = 0.00143$). For $PM_{2.5}$, the corresponding values are $R^2 = 0.349$ and $p = 0.0261$ for the linear regression, and $\rho = 0.745$ with $p = 0.00325$ for the Spearman correlation.

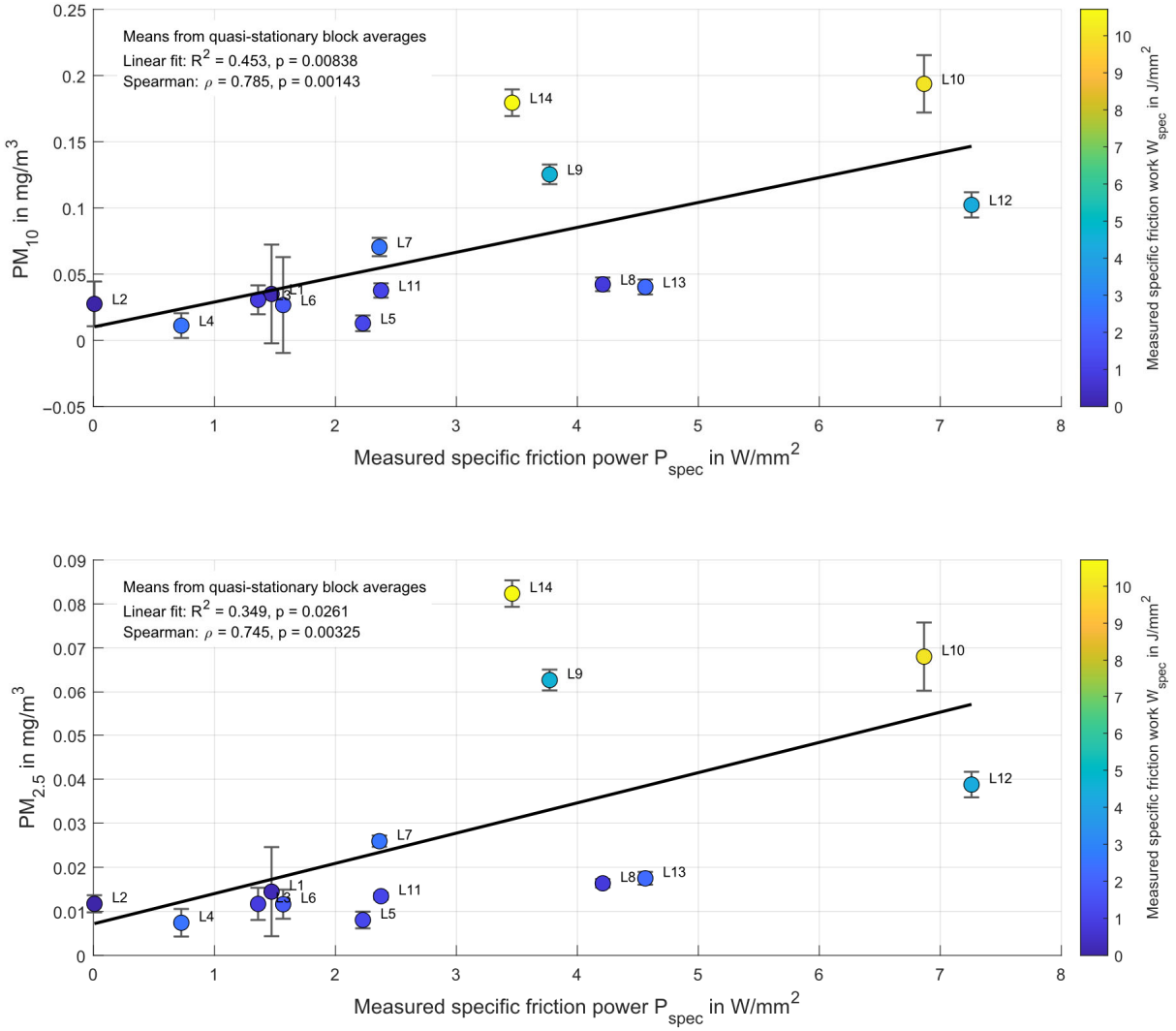

Figure 6. Quasi-stationary mean PM_{10} and $PM_{2.5}$ emissions of friction system F as a function of measured specific friction power. Means were calculated from cycles 21 onward using consecutive 20-cycle block averages; error bars indicate 95% confidence intervals. Point color indicates the corresponding measured specific friction work. Partly adapted from [24].

Compared with the evaluation over measured specific friction work, these results indicate that specific friction power captures the general trend of increasing emissions, but with clearly lower descriptive capability. In particular, load cases with comparable frictional power but different specific friction work still show substantial differences in PM_{10} and

$PM_{2.5}$ levels. This suggests that frictional power alone is not sufficient to uniquely describe the emission behavior of the investigated metallic friction system.

Across all investigated load stages, PM_{10} concentrations remain higher than $PM_{2.5}$ concentrations, while both fractions exhibit the same overall tendency with increasing frictional loading. Together with the stronger statistical relationship obtained for specific friction work, this supports the interpretation that specific friction work provides the more robust descriptor of emission intensity within the investigated operating range, whereas specific friction power should be regarded as an additional but less discriminating load parameter. These findings are consistent with the extended data set including friction paring B and C, where higher load stages associated with increased friction work systematically result in elevated PM_{10} and $PM_{2.5}$ emissions. In [22], load levels 4 and 5 similarly exhibit the highest particle concentrations for both organic friction systems, confirming the dominant role of frictional energy input across different material classes.

3.2. Influence of Friction Material Systems on Emissions (RQ3)

3.2.1. Organic Pad with C45 and GGG40 Counter Disc (A and B) vs. Organic Highly Abrasive Pad with C45 Steel Counter Disc (C)

Urbano et al. [22] investigated two organic ring-type friction pairings with identical pad geometry but different pad formulations and counter-disc materials, referred to as systems B and C. In the present study, this comparison is extended by including friction pairing A. Thus, the analysis now comprises an organic, mass-pressed pad without a reinforcement structure sliding against either a C45 steel or GGG40 cast iron counter disc, as well as system C, which consists of an organic, mass-pressed pad with a reinforcement structure and an increased abrasive fraction, resulting in a highly abrasive tribological behavior. To assess whether differences in particulate emissions can be directly attributed to differences in friction behavior, the mean friction coefficients of friction pairings A, B, and C were first compared across the investigated load stages (see Figure 7). For this purpose, the quasi-stationary regime from cycle 21 onward was evaluated using consecutive 20-cycle block averages in order to reduce the influence of early transient effects and cycle-to-cycle dependence.

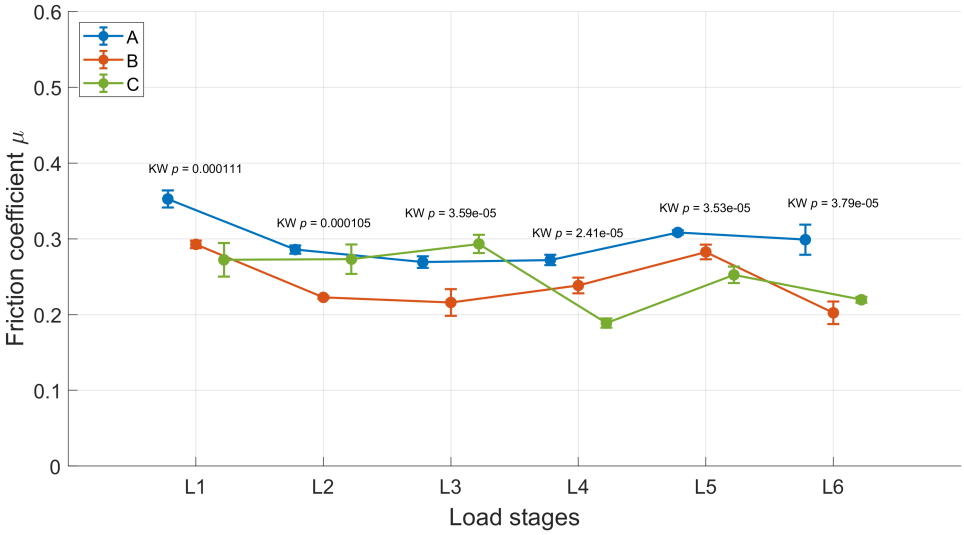

Figure 7. Comparison of the quasi-stationary friction coefficients of friction pairings A, B, and C across load stages. Mean values are based on consecutive 20-cycle block averages from cycle 21 onward; error bars indicate 95% confidence intervals.

As shown in Figure 7, the friction coefficients of pairings A, B, and C remain within a partially overlapping range across the investigated load stages. Non-parametric group

comparisons revealed significant differences between the three pairings for all load stages. However, the pairwise pattern of friction coefficient differences does not mirror the much stronger and more systematic separation observed for PM_{10} and $PM_{2.5}$. This indicates that the substantial differences in particulate emissions cannot be explained by the mean friction coefficient alone.

A comparison of the emitted particle mass nevertheless reveals pronounced differences between the investigated systems. In particular, friction pairing C exhibits markedly elevated PM_{10} and $PM_{2.5}$ emissions compared with pairings A and B across the investigated load stages (see Figure 8). The PM data were likewise evaluated in the quasi-stationary regime using consecutive 20-cycle block averages from cycle 21 onward. For both PM_{10} and $PM_{2.5}$, non-parametric group comparisons indicated significant differences between pairings A, B, and C in all investigated load stages. Pairwise comparisons with Holm correction showed that pairing C exhibited significantly higher PM levels than pairing B across all load stages for both particle fractions. In comparison with pairing A, pairing C also showed significantly elevated PM_{10} and $PM_{2.5}$ levels in nearly all load stages. By contrast, pairings A and B remained substantially closer to each other, with only isolated non-significant contrasts. These findings statistically confirm that pairing C forms a distinct high-emission system within the investigated organic friction pairings.

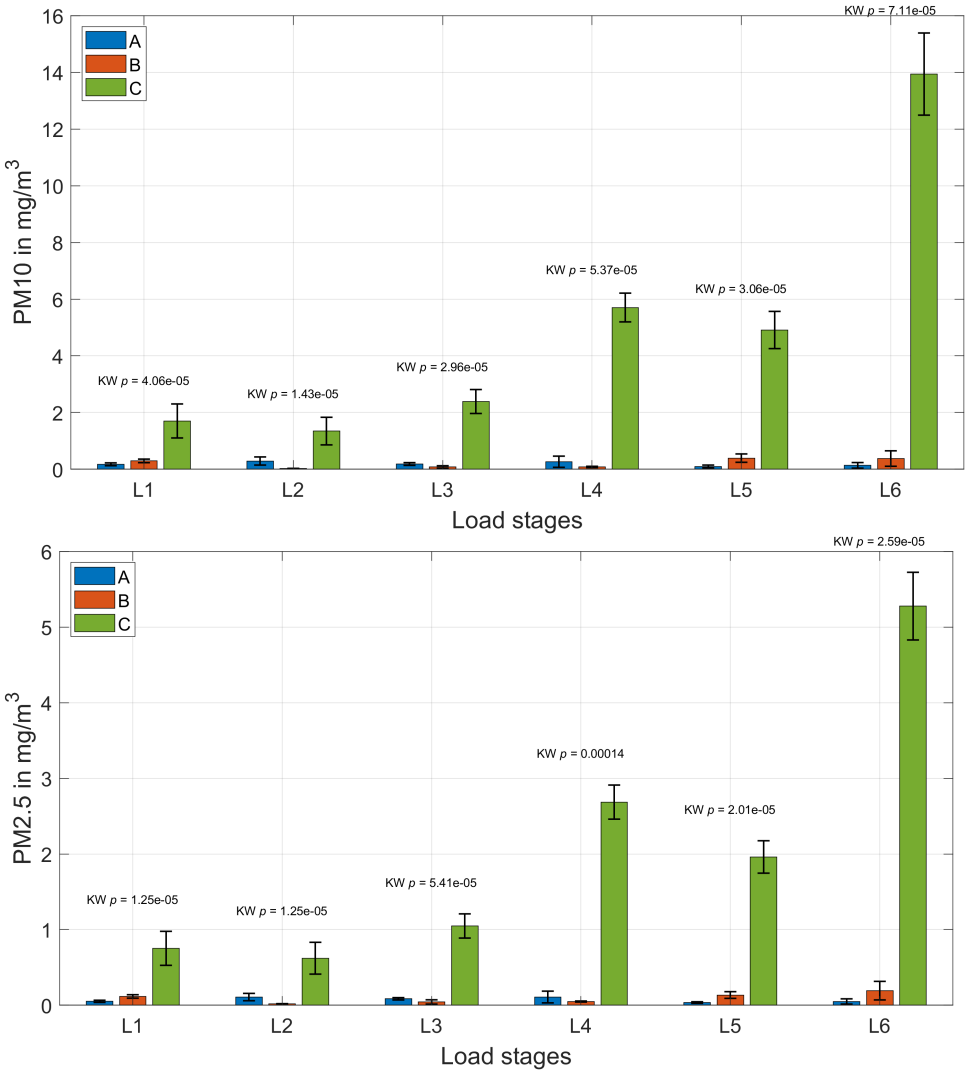

Figure 8. Comparison of quasi-stationary PM_{10} and $PM_{2.5}$ emissions for friction pairings A, B, and C across load stages. Mean values are based on consecutive 20-cycle block averages from cycle 21 onward; error bars indicate 95% confidence intervals. Partly adapted from [22].

Depending on the load stage, PM_{10} emissions from pairing C were approximately 5 to 49 times higher, while $PM_{2.5}$ emissions were about 6 to 35 times higher than those of pairings A and B. The gravimetric pad mass loss shown in Figure 9 also indicates markedly increased wear for pairing C in most load stages, particularly under the higher-load conditions L4 to L6. In load stage L2, pairing C still showed substantially higher mass loss than pairing B, although pairing A reached a similarly high level. Each wear value represents one tribological test condition, whereas the reported pad mass loss was obtained from five repeated weighing measurements of the same worn specimen to reduce measurement uncertainty. Overall, the comparison of Figures 8 and 9 suggests a qualitative correspondence between wear mass loss and airborne particle emissions, especially for pairings B and C. However, the relationship is not strictly proportional, because gravimetric wear quantifies the total removed pad mass, whereas the aerosol measurement captures only the airborne fraction within the measured PM size range. Part of the worn material may remain in the contact as third-body material, adhere to the counterface or surrounding surfaces, agglomerate into larger fragments outside the PM_{10} or $PM_{2.5}$ range, or settle before being detected as airborne aerosol. Accordingly, gravimetric wear and aerosolized particle release represent related but not identical response variables.

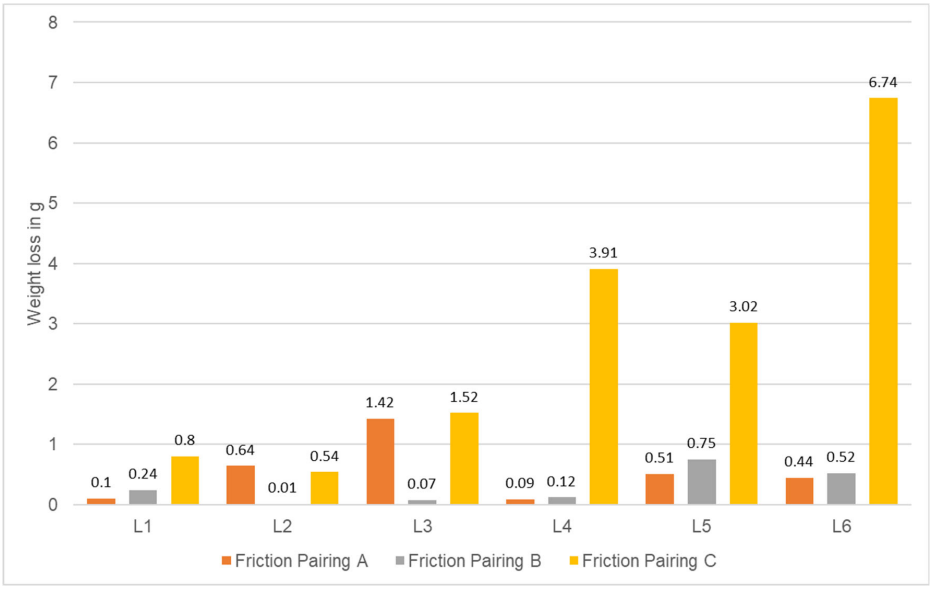

Figure 9. Weight loss after performed load stages for friction pairs A, B, and C.

Figure 10 shows the EDX analyses of collected PM_{10} particles of friction pairing C. The results revealed iron content in emissions from system C, although the pad itself is metal-free. This suggests an increased counter-disc contribution to the emitted particle mass. These results demonstrate that disc material and pad formula has a major influence on emissions even when pad geometry is identical. The combination of the abrasive organic pad with C45 (system C) leads to higher counterface wear, smoother disc surfaces and increased particle release compared to the combination with GGG40 (system B).

In Figure 11, two SEM images of PM_{10} deposits are shown for L1 (left) and L5 (right) case. In both images, the deposits are dominated by irregular, strongly agglomerated wear debris which is typical for mechanically generated brake wear particles. Furthermore, both cases experienced identical specific friction power, but differed in specific friction work with the L5 case experiencing a higher condition. As a result, L5 exhibits a tendency toward coarser and more compact agglomerates with more pronounced fragments locally. This indicates that there is an increased amount of cumulative material throughout the PM_{10}

fraction of the L5 case. No qualitative change in particle morphology (e.g., appearance of spherical melt-derived particles) is evident in both cases.

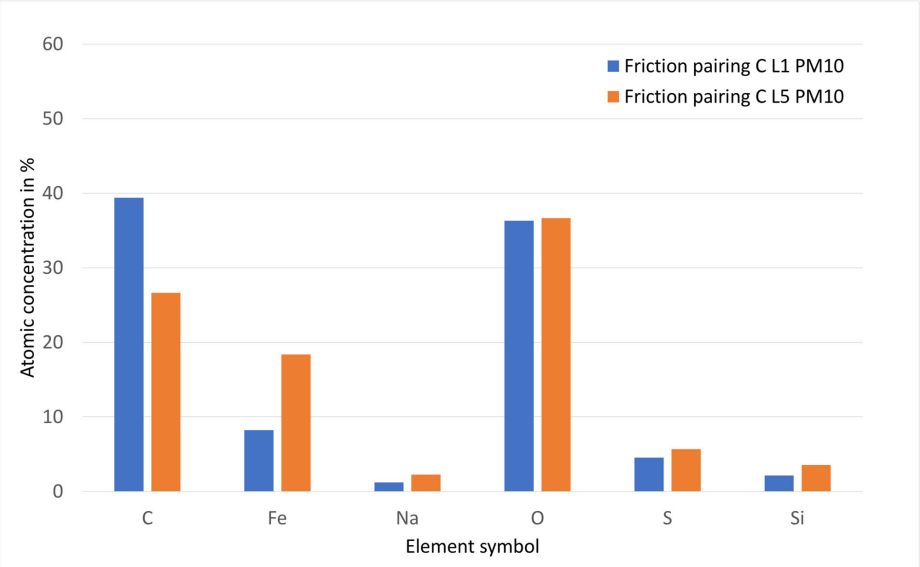

Figure 10. Atomic concentration of PM_{10} emissions of friction pairing C for load stages 1 and 5 determined by EDX analysis. Partly adapted from [22].

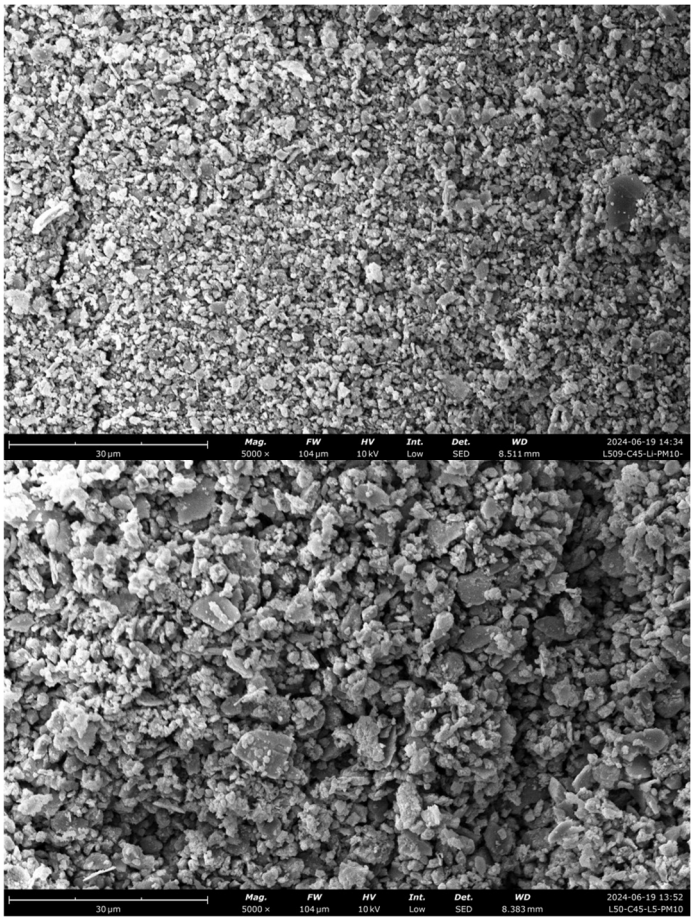

Figure 11. SEM images of PM_{10} deposits at identical specific friction power (top L1 and down L5).

3.2.2. Wound Glass Fiber-Reinforced Systems with Spring Features (D and E)

Another investigated brake-pad type consists of organic wound linings with glass fiber reinforcement, represented by systems D and E. Both systems include spring elements in their construction and differ primarily in the counter-disc material, with system D using a C45 steel counter disc and system E using a GGG40 cast iron counter disc. Figure 12 compares the quasi-stationary PM_{10} and $PM_{2.5}$ emissions of both systems across the investigated load stages. The evaluation was based on cycles 21 onward using consecutive 20-cycle block averages; error bars indicate 95% confidence intervals.

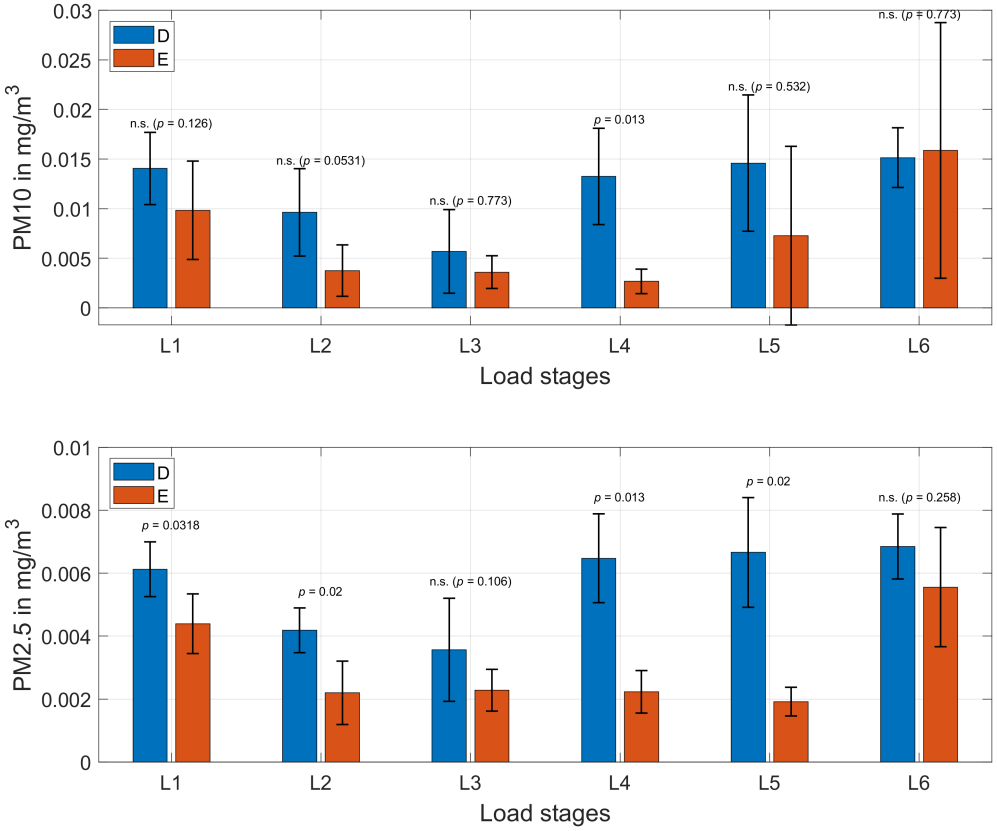

Figure 12. Quasi-stationary PM_{10} and $PM_{2.5}$ emissions of friction pairings D and E across load stages L1 to L6. Mean values were calculated from cycles 21 onward using consecutive 20-cycle block averages; error bars indicate 95% confidence intervals. Statistical annotations refer to Holm-corrected pairwise Wilcoxon rank-sum tests for D versus E within each load stage; n.s. denotes no statistically significant difference at alpha = 0.05.

Overall, both wound glass fiber-reinforced systems showed comparatively low emission levels relative to the organic ring-type systems discussed previously. However, the statistical comparison between D and E revealed a differentiated pattern. For $PM_{2.5}$, significant differences between both systems were found in load stages L1, L2, L4, and L5 after Holm correction, whereas no significant differences were observed in L3 and L6. For PM_{10}, a significant difference remained only in L4 after correction for multiple comparisons, while the remaining load stages did not show statistically robust separation. The friction coefficient differed significantly between D and E in most load stages, except for L3 (see Figure 13).

These results indicate that the two wound systems cannot be regarded as fully equivalent, but also do not show a uniform separation across all load stages and particle fractions. The comparatively low emission level of both systems is consistent with the compliant system design including spring elements. However, the differences between D and E cannot be attributed unambiguously to a single mechanistic factor on the basis of the present data.

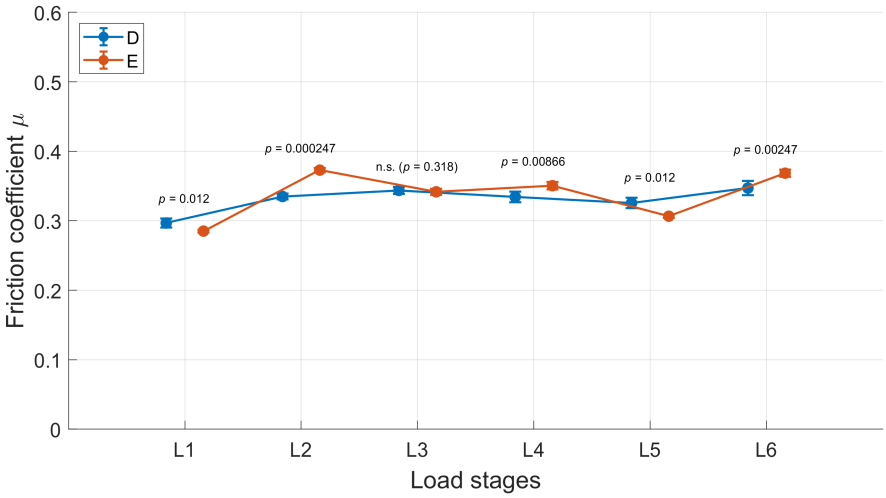

Figure 13. Quasi-stationary friction coefficients of friction pairings D and E across load stages L1 to L6. Mean values were calculated from cycles 21 onward using consecutive 20-cycle block averages; error bars indicate 95% confidence intervals. Statistical annotations refer to Holm-corrected pairwise Wilcoxon rank-sum tests for D versus E within each load stage; n.s. denotes no statistically significant difference at alpha = 0.05.

4. Discussion

4.1. Application-Relevant and Mechanistically Interpretable Capture of Brake Wear Particle Emissions

RQ1 addressed how a dry friction test bench can be used to capture application-relevant brake wear particle emissions in a quantitatively robust and mechanistically interpretable manner with respect to particle mass, size, and chemical composition. The present results show that the developed methodology provides such a test environment under controlled, tribologically relevant operating conditions. PM_{10} and $PM_{2.5}$ emissions were measured reproducibly over repeated braking sequences, while friction coefficient, temperature, and gravimetric wear were recorded in parallel. In addition, size-resolved aerosol measurements and SEM/EDX-based particle characterization enabled the emitted material to be interpreted not only in terms of concentration, but also with respect to particle size and chemical composition.

The measurement sequence further revealed an early transient phase with elevated PM levels and stronger cycle-wise drift, followed by a more stable quasi-stationary regime. The additional evaluation from cycle 21 onward therefore strengthens the quantitative robustness of the statistical interpretation and demonstrates that the test bench is sufficiently sensitive to resolve time-dependent adaptation processes in the friction contact.

In this context, application relevance refers to the controlled reproduction of tribologically relevant load states rather than to full vehicle-level equivalence. The test bench therefore represents a reduced but physically interpretable experimental environment for investigating brake wear particle formation. Accordingly, RQ1 can be answered positively: the dry friction test bench enables application-relevant, quantitatively robust, and mechanistically interpretable capture of brake wear particle emissions when particle mass, size-resolved aerosol information, and chemical particle characterization are evaluated together.

4.2. RQ2: Influence of Operating Parameters

The consolidated results confirm that within the investigated operating range of friction system F, specific friction work is a physically meaningful and robust descriptor for brake wear particle emissions in dry-running friction systems. For system F, PM_{10} and

$PM_{2.5}$ emissions increase significantly with specific friction work over the investigated range of load stages. When the evaluation is restricted to the quasi-stationary regime from cycle 21 onward and based on consecutive 20-cycle block averages, both particle fractions show a strong positive statistical relationship with measured specific friction work.

Specific friction power, by contrast, exhibits a weaker but still relevant association. While high power densities promote elevated emissions, especially of finer fractions, the scatter observed within the operating range of system F suggests that additional factors such as thermal diffusivity, contact compliance, and tribofilm stability modulate the effect of power density.

The independent effect of contact pressure on emissions appears difficult to isolate when specific friction work is kept constant. The present design indicates that contact pressure contributes to the emission response together with sliding velocity, inertial loading, and the resulting tribological energy input, but it does not yet permit a strict separation of their independent main effects. A main influence of pressure is observed on emission stability: higher pressures often stabilize the third-body layer, reduce short-term fluctuations, and suppress extreme peaks, whereas low-pressure, high-speed conditions are prone to unstable contact and highly variable emissions.

Overall, RQ2 can be answered as follows: sliding velocity and inertial load, as reflected in the resulting specific friction work, are the dominant operating parameters governing PM_{10} and $PM_{2.5}$ emission intensity within the investigated range of friction system F. Contact pressure primarily affects the temporal structure and stability of the emissions rather than their absolute level, while specific friction power serves as a useful but less discriminating descriptor. However, future work should isolate the individual effects of sliding velocity, contact pressure, and temperature in more detail, as specific friction work represents a resulting rather than a direct operating parameter. This is particularly relevant for assessing whether, at identical levels of specific friction work, variations in sliding velocity and contact pressure differ in their influence on particle emissions.

4.3. RQ3: Influence of Friction Material Systems

4.3.1. Influence of Friction System Configuration on Particle Emissions

The comparison of different friction pairings shows that the friction system strongly influences particle emissions even under identical operating conditions. The organic ring systems A and B, which differ only in the counter-disc material (C45 versus GGG40), demonstrate that the counter-disc material alone can modify emission levels across the load stages. However, the resulting PM_{10} and $PM_{2.5}$ concentrations remain within the same overall emission range.

The high-abrasive organic system C exhibits the highest particle emissions among the organic pads. This observation is now statistically supported by the quasi-stationary block-based evaluation: for PM_{10} and $PM_{2.5}$, significant differences between pairings A, B, and C were found across all investigated load stages, and pairing C consistently formed the high-emission system, especially relative to pairing B and, in nearly all load stages, also relative to pairing A. This behavior confirms that an increased abrasive character and reinforcement-related system stiffness promote a more aggressive interaction with the counterface and enhanced particle release. The intensified disc interaction is corroborated by SEM/EDX analysis, which reveals an increased iron content in the emitted particles.

At the same time, the friction-coefficient comparison of A, B, and C shows that the three systems remain within a partially overlapping range, although statistically significant pairwise differences occur in many load stages. Importantly, this friction-coefficient pattern does not mirror the much stronger and more systematic separation observed for PM_{10}

and $PM_{2.5}$. The pronounced emission differences between A, B, and C therefore cannot be explained by the mean friction coefficient alone.

The wound glass fiber-reinforced systems D and E show that constructive measures such as spring features and improved compliance are associated with reduced emissions. Despite comparable operating conditions, these systems exhibit comparatively low PM_{10} and $PM_{2.5}$ levels. However, the statistical comparison between D and E reveals a differentiated rather than a uniform picture: for $PM_{2.5}$, significant differences were found in several load stages, whereas for PM_{10} only isolated load stages remained significant after correction for multiple comparisons. Thus, D and E cannot be regarded as fully equivalent, but neither do they show a consistent separation across all load stages and particle fractions. This underlines the importance of mechanical compliance and homogeneous stress distribution for emission control, while also showing that the present data do not permit a strict attribution of the observed behavior to a single constructive mechanism such as improved load distribution alone.

The sintered metallic system F behaves differently due to its metallic matrix brake pad with high thermal capacity, but still follows the general trend of emissions scaling with friction work.

Given that pad geometry and material formulation were not varied independently in the present matrix, geometry is treated as part of the overall friction system. It is therefore not possible to derive isolated geometric trends. However, the consistent differences between ring-shaped and segment-shaped systems and between non-spring-supported and spring-supported pads support the view that geometric and constructive design can be powerful levers when combined with suitable material formulations.

4.3.2. Key Findings

The main findings can be summarized as follows. First, the friction material system has a decisive influence on PM_{10} and $PM_{2.5}$ emissions. Second, the counter-disc material can alter the emission level even when the pad material remains unchanged. Third, highly abrasive organic systems tend to promote increased particle release. Fourth, constructive features that improve compliance are associated with comparatively low emission levels, although their isolated contribution cannot yet be quantified independently from the overall system design. Overall, the results indicate that particle emission behavior is governed by the interaction of pad formulation, reinforcement structure, constructive design, and counter-disc material rather than by a single isolated factor.

4.3.3. Recommendations for Reducing Particle Emissions

Based on the present results, several recommendations for reducing particle emissions can be derived. From a constructive point of view, mechanically compliant pad designs with improved load distribution, for example through spring-supported concepts, appear beneficial. From a material perspective, highly abrasive pad formulations should be avoided if low particle emissions are the primary objective. In addition, the counter-disc material should be selected carefully, as it can significantly modify the emission behavior. Overall, emission reduction should be addressed at the level of the complete friction system, including pad formulation, reinforcement structure, constructive features, and counter-disc material.

4.3.4. Answer to RQ3

Thus, RQ3 can be answered as follows: friction material systems, defined by pad formulation, reinforcement structure, constructive features, and counter-disc material, have a decisive impact on PM_{10} and $PM_{2.5}$ emissions. Organic high-abrasive systems and

combinations with C45 discs tend to increase emissions, while wound, compliant pads and suitable counter-disc materials reduce them.

4.4. Emissions as Catalysts for Wear- and Mechanism-Based Modeling

A qualitative correspondence between particle mass concentrations and gravimetric wear mass loss could be observed, particularly for friction pairings B and C. However, this relationship was not strictly proportional across all investigated systems and load stages. This indicates that gravimetric wear and aerosolized particle release represent related but not identical response variables. PM measurements cannot therefore be interpreted as a direct one-to-one proxy for total wear progression in dry-running friction systems. In combination with SEM/EDX-based identification of particle origin and chemical composition, they nevertheless provide valuable complementary information for understanding tribological system behavior and emission formation.

The present results establish a validated experimental basis for data-driven and hybrid modeling approaches aiming to predict PM_{10} and $PM_{2.5}$ emissions as a function of operating parameters and friction pairing. In particular, the dominant role of specific friction work within system F, the statistically confirmed separation of the organic systems A, B, and C, and the low-emission behavior of the wound systems D and E constitute key constraints and validation targets for future predictive models.

4.5. Methodological Limitations

Geometry and material composition are coupled in the presented matrix. The organic ring pads (A/B) and the high-abrasive ring pad (C) share a ring geometry but differ in formulation. The wound pads (D/E) combine geometry changes with spring features and reinforcement, and the sintered pad (F) is segment-shaped. No material is available in multiple geometries, and geometry is therefore treated as part of the friction system rather than an independent variable. Consequently, geometric influences cannot be isolated and are discussed as system effects.

In addition, the statistical evaluation is based on quasi-stationary block averages rather than on the assumption that all braking cycles are fully independent replicates. The first 20 cycles were excluded in the additional statistical evaluation because the early part of the sequence frequently showed elevated PM levels and stronger cycle-wise drift, indicating a transient regime. The selected threshold is therefore empirical and intended to separate early transient behavior from the subsequent quasi-stationary response.

The gravimetric wear values were obtained as condition-level mass differences. Repeated weighing was used to reduce measurement uncertainty, but these repeated weighing measurements do not constitute independent tribological replicates. Wear results are therefore interpreted descriptively and in relation to PM trends, rather than on a fully replicated inferential data basis.

Finally, the present setup represents a controlled tribological test environment rather than a full vehicle brake system. The methodology reproduces tribologically relevant operating states, but it does not include all boundary conditions of a real brake application, such as vehicle-specific ventilation, environmental humidity variation, regenerative braking interaction, and full driving-cycle dynamics. The results should therefore be interpreted as physically meaningful trends under controlled application-relevant frictional conditions rather than as direct one-to-one predictions of vehicle-level non-exhaust emissions.

5. Conclusions

Non-exhaust particulate matter emissions from brake systems remain a major contributor to traffic-related PM_{10} and $PM_{2.5}$, particularly as exhaust emissions are progressively

reduced by regulation. While numerous studies have addressed individual aspects of brake wear particle formation, the combined influence of operating parameters and friction material systems, as well as their mechanistic interpretation, has remained insufficiently investigated. This work establishes a dry-friction-test-bench-based measurement methodology for capturing brake wear particle emissions under controlled, tribologically relevant operating conditions in a manner that is quantitatively robust and mechanistically interpretable with respect to particle mass, size, and chemical composition. The results show that, when combined with aerosol-based PM measurement, size-resolved analysis, tribological state variables, and SEM/EDX characterization, the methodology enables a differentiated assessment of how operating conditions and friction-system design affect particulate emissions from dry-running friction systems.

The main conclusions of this study can be summarized as follows:

1. The developed methodology provides an application-relevant and mechanistically interpretable experimental framework for analyzing brake wear particle emissions in dry-running friction systems. Application relevance in this context refers to the controlled reproduction of tribologically relevant load states rather than to full vehicle-level equivalence.
2. Within the investigated operating range of friction system F, specific friction work is the clearest and most robust descriptor of PM_{10} and $PM_{2.5}$ emission intensity. Its relationship with both particle fractions remains strong when the analysis is restricted to the quasi-stationary regime and based on block-averaged data.
3. Sliding velocity and inertial loading contribute strongly to the emission response through their effect on the resulting frictional energy input. Contact pressure is also relevant, but its independent contribution could not yet be isolated strictly in the present design. The data indicate that it influences not only emission level, but also the temporal stability of the emission response.
4. Specific friction power provides additional insight but shows a weaker and more system-dependent association and is less discriminating than specific friction work within the investigated range.
5. The comparison of the organic ring-type systems A, B, and C statistically confirms that friction-system design has a decisive influence on PM_{10} and $PM_{2.5}$ emissions. Pairing C forms a distinct high-emission system, whereas A and B remain substantially closer to one another. The corresponding friction coefficients remain only partially overlapping and do not mirror the much stronger separation observed for PM emissions.
6. The wound, spring-supported systems D and E exhibit comparatively low emission levels overall. However, their comparison reveals a differentiated pattern rather than a uniform separation across all load stages and particle fractions, especially after correction for multiple comparisons.
7. A qualitative correspondence between gravimetric wear and airborne particle emissions can be observed, particularly for friction pairings B and C. However, the relationship is not strictly proportional across all investigated systems and conditions, indicating that total material removal and aerosolized particle release are related but not identical response variables.
8. Pad geometry and constructive design cannot be isolated from material effects in the present test matrix and are therefore treated as part of the friction system. Future studies should include systematic variation in geometry with constant material as well as a stricter separation of sliding velocity, contact pressure, and thermal effects in order to isolate their individual contributions more clearly

Overall, this work provides a tribologically relevant, methodologically consistent, and statistically strengthened framework for analyzing brake wear particle emissions from dry-

running friction systems such as brake and clutch systems. By linking operating conditions, frictional energy input, friction-system characteristics, and particle properties including mass, size, and chemistry, the study contributes to a more differentiated understanding of emission formation mechanisms. The results offer a solid experimental basis for the design of low-emission friction systems and for the development and validation of data-driven and hybrid predictive models for PM_{10} and $PM_{2.5}$ emissions in the context of future non-exhaust emission regulation.

Author Contributions: Conceptualization, F.P.U. and A.A.; Methodology, F.P.U. and A.A.; Validation, F.P.U.; Formal analysis, F.P.U.; Investigation, F.P.U.; Resources, S.O. and A.A.; Data curation, F.P.U.; Writing—original draft, F.P.U.; Writing—review & editing, A.B., S.O. and A.A.; Visualization, F.P.U.; Supervision, A.B. and A.A.; Funding acquisition, A.A. All authors have read and agreed to the published version of the manuscript.

Funding: This research was partly funded by the German Federal Ministry for Economic Affairs and Energy though AiF within the program for Industrial Collective Research (IGF) grant number 22080-N and the APC was funded by KIT Publication Fund.

Supported by:

Federal Ministry
for Economic Affairs
and Climate Action

on the basis of a decision
by the German Bundestag

Data Availability Statement: The data presented in this study are available on reasonable request from the corresponding author. The raw measurement data are not publicly available due to project-specific confidentiality and release restrictions.

Conflicts of Interest: The authors declare no conflicts of interest.

Abbreviations

The following abbreviations are used in this manuscript:

PM	Particulate Matter
PM_{10}	Particulate Matter with aerodynamic diameter < 10 µm
$PM_{2.5}$	Particulate Matter with aerodynamic diameter < 2.5 µm
C45	Medium-carbon steel
GGG40	Cast iron with spheroidal graphite
DOE	Design of Experiments
SEM	Scanning Electron Microscopy
EDX	Energy-Dispersive X-ray Spectroscopy

References

1. Grigoratos, T.; Martini, G. Brake wear particle emissions: A review. *Environ. Sci. Pollut. Res. Int.* **2015**, *22*, 2491–2504. [CrossRef] [PubMed]
2. Amato, F.; Cassee, F.R.; van der Denier Gon, H.A.C.; Gehrig, R.; Gustafsson, M.; Hafner, W.; Harrison, R.M.; Jozwicka, M.; Kelly, F.J.; Moreno, T.; et al. Urban air quality: The challenge of traffic non-exhaust emissions. *J. Hazard. Mater.* **2014**, *275*, 31–36. [CrossRef] [PubMed]
3. Joint Research Centre: Institute for Energy and Transport. *Non-Exhaust Traffic Related Emissions—Brake and Tyre Wear PM—Literature Review*; Publications Office of the European Union: Luxembourg, 2014.
4. Belis, C.A.; Karagulian, F.; Larsen, B.R.; Hopke, P.K. Critical review and meta-analysis of ambient particulate matter source apportionment using receptor models in Europe. *Atmos. Environ.* **2013**, *69*, 94–108. [CrossRef]
5. Wahlström, J. Special Issue Editorial: Study of Brake Wear Particle Emissions. *Atmosphere* **2020**, *11*, 1359. [CrossRef]

6. Kukutschová, J.; Roubíček, V.; Malachová, K.; Pavlíčková, Z.; Holuša, R.; Kubačková, J.; Mička, V.; MacCrimmon, D.; Filip, P. Wear mechanism in automotive brake materials, wear debris and its potential environmental impact. *Wear* **2009**, *267*, 807–817. [CrossRef]
7. Liati, A.; Schreiber, D.; Lugovyy, D.; Gramstat, S.; Dimopoulos Eggenschwiler, P. Airborne particulate matter emissions from vehicle brakes in micro- and nano-scales: Morphology and chemistry by electron microscopy. *Atmos. Environ.* **2019**, *212*, 281–289. [CrossRef]
8. Gomes Nogueira, A.P. Particulate Matter Emission Issues in Brake Systems. Ph.D. Thesis, University of Trento, Trento, Italy, 2022.
9. Kukutschová, J.; Moravec, P.; Tomášek, V.; Matějka, V.; Smolík, J.; Schwarz, J.; Seidlerová, J.; Šafářová, K.; Filip, P. On airborne nano/micro-sized wear particles released from low-metallic automotive brakes. *Environ. Pollut.* **2011**, *159*, 998–1006. [CrossRef] [PubMed]
10. Men, Z.; Zhang, X.; Peng, J.; Zhang, J.; Fang, T.; Guo, Q.; Wei, N.; Zhang, Q.; Wang, T.; Wu, L.; et al. Determining factors and parameterization of brake wear particle emission. *J. Hazard. Mater.* **2022**, *434*, 128856. [CrossRef] [PubMed]
11. Chandra Verma, P.; Menapace, L.; Bonfanti, A.; Ciudin, R.; Gialanella, S.; Straffelini, G. Braking pad-disc system: Wear mechanisms and formation of wear fragments. *Wear* **2015**, *322–323*, 251–258. [CrossRef]
12. Wang, Y.; Li, A.; Yin, H.; Su, S.; Lai, Y.; Chen, W.; Wang, X.; Tan, J.; Hao, L.; Shuai, S.; et al. Brake wear particles from various temperatures: Emission characteristics, generation processes and evolutions. *Emerg. Contam.* **2025**, *11*, 100554. [CrossRef]
13. Sutschet, A.; Bause, K.; Bischofberger, A.; Ott, S. Feinstaubemissionen trockenlaufender Friktionssysteme in Fahrzeugen. *Forsch Ingenieurwes.* **2023**, *87*, 521–528. [CrossRef]
14. Straffelini, G.; Gialanella, S. Airborne particulate matter from brake systems: An assessment of the relevant tribological formation mechanisms. *Wear* **2021**, *478–479*, 203883. [CrossRef]
15. Hao, Y.; Deng, S.; Yang, Y.; Song, W.; Tong, H.; Qiu, Z. Chemical Composition of Particulate Matter from Traffic Emissions in a Road Tunnel in Xi'an, China. *Aerosol Air Qual. Res.* **2019**, *19*, 234–246. [CrossRef]
16. Candeo, S.; Leonardi, M.; Gialanella, S.; Straffelini, S. Influence of contact pressure and velocity on the brake behaviour and particulate matter emissions. *Wear* **2023**, *514–515*, 204579. [CrossRef]
17. Alemani, M.; Wahlström, J.; Olofsson, U. On the influence of car brake system parameters on particulate matter emissions. *Wear* **2018**, *396–397*, 67–74. [CrossRef]
18. Zhang, Q.; Fang, T.; Men, Z.; Wei, N.; Peng, J.; Du, T.; Zhang, X.; Ma, Y.; Wu, L.; Mao, H. Direct measurement of brake and tire wear particles based on real-world driving conditions. *Sci. Total Environ.* **2024**, *906*, 167764. [CrossRef] [PubMed]
19. Vasiljević, S.; Lukić, J.; Miloradović, D.; Glišović, J. Driving cycles for studying brake wear particle emissions on an inertial brake dynamometer. *Tribol. Mater.* **2023**, *2*, 8–19. [CrossRef]
20. Kreider, M.L.; Panko, J.M.; McAtee, B.L.; Sweet, L.I.; Finley, B.L. Physical and chemical characterization of tire-related particles: Comparison of particles generated using different methodologies. *Sci. Total Environ.* **2010**, *408*, 652–659. [CrossRef] [PubMed]
21. Vasiljević, S.; Glišović, J.; Lukić, J.; Miloradović, D.; Stanojević, M.; Đorđević, M. Analysis of Parameters Influencing the Formation of Particles during the Braking Process: Experimental Approach. *Atmosphere* **2023**, *14*, 1618. [CrossRef]
22. Urbano, F.P.; Bause, K.; Bischofberger, A.; Ott, S.; Albers, A. Particulate matter emissions in brake systems—Development and application of an extended measurement methodology for particulate matter emissions from dry-running friction systems. *Tribol. Schmier.* **2024**, *71*, 19–25. [CrossRef]
23. Albers, A.; Urbano, F.P.; Bause, K.; Bischofberger, A.; Ott, S. *Verschleißpartikelmessung im Trockenlauf: Entwicklung Einer Methode zur Verschleißpartikelmessung Trockenlaufender Kupplungssysteme*; Abschlussbericht FVA-Nr. 955 I; FVA Forschungsvereinigung Antriebstechnik e.V.: Frankfurt, Germany, 2025.
24. Urbano, F.P.; Bischofberger, A.; Albers, A. Partikelemissionen in trockenlaufenden Friktionssystemen: Einfluss von Betriebsparametern und Material auf die Feinstaubemissionen von Bremssystemen. In *Kupplungs- und Bremssysteme für Mobile und Stationäre Anwendungen, VDI-Fachtagung: Systeme—Methoden—Anwendungen: 21. und 22. Mai 2025, Karlsruhe*; VDI Wissensforum GmbH, Ed.; VDI Verlag Gmbh: Düsseldorf, Germany, 2025; pp. 193–211.